

# Electrocatalytic activity of Pt nanoparticles supported on novel functionalized reduced graphene oxide-chitosan for methanol electrooxidation

Mehri-Saddat Ekrami-Kakhki<sup>1</sup> · Nahid Farzaneh<sup>1</sup> · Sedigheh Abbasi<sup>1</sup> · Batoul Makiabadi<sup>2</sup>

Received: 6 January 2017 / Accepted: 2 May 2017 / Published online: 10 May 2017  
© Springer Science+Business Media New York 2017

**Abstract** Here, graphene oxide (GO) was synthesized by a modified Hummers' method and was functionalized with 1,1'-dimethyl-4,4'-bipyridinium dichloride (MV) accompanied by chitosan (CH) to prepare a novel MV-RGO-CH support. Pt/MV-RGO-CH catalyst was prepared by immobilization of the Pt nanoparticles on MV-RGO-CH support. The microstructure and morphology of the prepared catalyst was characterized by transmission electron microscopy and X-ray powder diffraction analysis. The electrocatalytic activity of Pt/MV-RGO-CH catalyst was investigated for methanol electrooxidation through cyclic voltammetry (CV), CO<sub>ads</sub> stripping voltammetry, chronoamperometry, and electrochemical impedance spectroscopy (EIS) techniques. The effects of some experimental factors for methanol electrooxidation such as methanol concentration, scan rate and temperature were studied at the prepared catalyst. Durability of the catalyst was also investigated. Comparing the catalytic activity of the Pt/MV-RGO-CH nanocatalyst with Pt/CH and Pt/MV-RGO catalysts indicated that Pt/MV-RGO-CH has a very good catalytic activity for methanol electrooxidation.

## 1 Introduction

Due to the environmental pollution of fossil fuels combustion and the increasing needs of energy, extensive research

has been done to find renewable and clean energy sources. Among different energy sources, direct methanol fuel cells (DMFCs) have been widely investigated as novel energy resources that produce electrical energy directly from chemical energy [1, 2]. Because of their low pollution, high efficiency, light weight and easy handling of the liquid methanol fuel, DMFCs have attracted a lot of attention [3]. Various catalytic materials have been investigated for methanol oxidation reaction (MOR), as interest in developing direct methanol fuel cell has risen. Platinum (Pt) has a high catalytic activity for MOR and is extensively utilized as anode material in DMFCs. However, the high cost of Pt catalyst and its easy poisoning with carbon monoxide, the intermediate of methanol oxidation, limit its application in DMFCs [4]. To improve the activity and stability of catalysts and to minimize the use of precious metals, particularly Pt [5–7], many carbon-based materials such as carbon nanofibers [8], carbon nanotubes (CNTs) [9–13], Vulcan XC-72 carbon [14, 15], mesoporous carbon [16, 17] and graphene [18–22] have been used as catalyst support.

Graphene has been extensively used as a catalyst support to improve the catalytic properties of catalysts, due to its high electronic conductivity, high specific surface area [23], ease of functionalization [24], and high charge mobility [25]. However, because of the chemical inertness of graphene nanosheets, its application has been limited [26, 27]. Graphene nanosheets can be produced by chemical reduction of the graphene oxide (GO). Reduced graphene oxide (RGO), rather than graphene, is usually utilized as supporting materials in fuel cells, because of the presence of functional groups like epoxide, carbonyl, hydroxyl and carboxyl groups on RGO which facilitate the dispersion of metal nanoparticles [28]. However, reduction of the graphene oxide decreases its surface area and prevents from good dispersion of the

✉ Mehri-Saddat Ekrami-Kakhki  
ekrami@esfarayen.ac.ir

<sup>1</sup> Nano Technology Laboratory, Engineering Department, Esfarayen University of Technology, Esfarayen, Iran

<sup>2</sup> Department of Chemical Engineering, Sirjan University of Technology, Sirjan, Iran

metal nanoparticles [29]. To overcome these drawbacks, RGO is non-covalently functionalized. Non-covalently functionalization of graphene prevents from the destruction of its electronic characteristics [30]. For example, Surface of graphene has been functionalized with poly (*N*-vinyl-2-pyrrolidone) [31], poly sodium styrene sulfonate [32], Nile blue [33] and toluidine blue [34]. Ma and coauthors [35] non-covalently functionalized graphene with 1,1'-dimethyl-4,4'-bipyridinium dichloride (methyl viologen) for good dispersion of the Pt nanoparticles. Recently, Qudsia and coauthors functionalized reduced graphene oxide with an aromatic compound 4-hydroxy-4'-*n*-pentylbiphenyl by an esterification reaction [36]. Sakho and coauthors used 1-pyrenecarboxylic acid for non-covalently functionalization of the reduced graphene oxide [37].

Here, the use of methyl viologen functionalized graphene sheets accompanied by chitosan polymer (MV-RGO-CH) was reported as a novel catalyst support for methanol electrooxidation. Chitosan (CH) which is produced by deacetylation of chitin is a biopolymer with a strong affinity for transition metals [38]. Functionalization of the reduced graphene oxide with chitosan and methyl viologen significantly improved the catalytic properties of the Pt catalyst for MOR. The electrocatalytic activity of the Pt/MV-RGO-CH catalyst was studied for methanol oxidation (MO) through cyclic voltammetry (CV), CO stripping, electrochemical impedance spectroscopy (EIS), and chronoamperometry techniques. The catalytic activity of the Pt/MV-RGO-CH catalyst for MO was also compared with that of Pt/CH and Pt/MV-RGO catalysts. The effects of some experimental factors such as scan rate, methanol concentration, and temperature were studied on the anodic current density and potential of MO at Pt/MV-RGO-CH catalyst. The durability investigation of this catalyst was also done.

## 2 Materials and methods

Graphene oxide nanosheets were synthesized according to the modified hummer's method using HNO<sub>3</sub>, H<sub>2</sub>SO<sub>4</sub> (98%), H<sub>2</sub>O<sub>2</sub> (30%), KMnO<sub>4</sub> (99% for analysis), graphite powder (99.5%), and HCl (37%) purchased from Merck. 1,1'-dimethyl-4,4'-bipyridinium dichloride (methyl viologen, i.e. MV 98% Sigma Aldrich) and NaBH<sub>4</sub> (96% Merck) were used for the synthesis of MV-RGO. Pt nanoparticles were prepared using hexachloroplatinic acid (H<sub>2</sub>PtCl<sub>6</sub>) from Merck. Chitosan ([2-amino-2-deoxy-(1-4)-β-D-glucopyranose], with medium molecular weight, 400,000 Da) was purchased from Fluka and dissolved in 1% acetic acid (glacial, 100% Merck) solution. Methanol (CH<sub>3</sub>OH, 99.2%, Merck) was used to investigate MOR.

### 2.1 Preparation of graphene oxide (GO)

GO nanosheets were prepared from graphite powder through a modified Hummers' method [39]. Typically, 25 ml HNO<sub>3</sub> and 75 ml H<sub>2</sub>SO<sub>4</sub> acids were mixed with 2.5 g graphite powder and vigorously stirred for 24 h. It was centrifuged to remove its acids and was dried at 60 °C. The dried powder was mixed with 25 ml acetone in a beaker and sonicated for about 30 min. After drying, 115 ml H<sub>2</sub>SO<sub>4</sub> was added to the mixture and stirred using magnet. Then 15 g KMnO<sub>4</sub> was added to the beaker very slowly in the presence of an ice bath. After the slow addition of 200 ml deionized water, 50 ml H<sub>2</sub>O<sub>2</sub> was added to the beaker. The mixture was centrifuged with HCl 5% aqueous solution, washed with water and dried at 60 °C. Finally it was characterized and used as GO.

### 2.2 Preparation of MV-RGO

MV-RGO was prepared through the chemical reduction of GO in the presence of MV using NaBH<sub>4</sub> as the reducing agent [35, 40]. Typically, 5 mL of the GO dispersion (11 mg mL<sup>-1</sup>) was diluted to the volume of 200 ml with deionized water and sonicated for about 1 h. 0.0178 g of MV was dissolved in 20 ml deionized water and added to the GO solution. After the addition of 0.33 g NaBH<sub>4</sub> to the solution, it was stirred for 24 h, centrifuged, washed with deionized water and dried at 60 °C. The black powder was MV-RGO.

### 2.3 Preparation of Pt/MV-RGO-CH nanocatalyst

To prepare Pt/MV-RGO-CH nanocatalyst, the following steps were followed. 1 mg MV-RGO was dispersed in 17.5 ml deionized water and 2.5 ml chitosan and sonicated for 1 h. 25 μl H<sub>2</sub>PtCl<sub>6</sub> solution was added to the mixture to prepare H<sub>2</sub>PtCl<sub>6</sub> 0.00125 M solution. Having been stirred for 1 h, 50 μl NaBH<sub>4</sub> (3 M) was added to the mixture as the reducing agent. The mixture was stirred for another 24 h, and then centrifuged to remove excess NaBH<sub>4</sub>. Pt-MV-RGO-CH was purified by several centrifugation and washing processes. It was finally dried at 60 °C for 12 h.

### 2.4 Preparation of GC/Pt/MV-RGO-CH electrode

The catalyst ink was prepared by ultrasonically redispersing 2 mg of the catalyst powder in 500 μl chitosan solution. Then, 5 μl of the prepared Pt/MV-RGO-CH ink was spread onto the glassy carbon electrode substrate and dried at room temperature.

## 2.5 Characterization

The size and dispersion of Pt nanoparticles were observed with TEM images taken with a Philips CM120 transmission electron microscope with the resolution  $\sim 2.5$  Å. The electrochemical characterization of Pt/MV-RGO-CH nanocomposite was done with a potentiostat/galvanostat Autolab (Nova software model PGSTAT 302 N, Metrohm, Netherlands) apparatus. A conventional three-electrode cell was used with a saturated calomel electrode (SCE) as the reference electrode. A platinum and a glassy carbon (GC) electrodes were used as the counter and working electrodes, respectively. Before the experiment, GC electrode was polished and sonicated in water and absolute ethanol. Afterwards, it was cleaned and activated in  $1.0 \text{ mol L}^{-1} \text{ H}_2\text{SO}_4$

solution by cyclic voltammetry (CV) technique between  $-1.5$  and  $+1.5$  V.

## 3 Results and discussion

### 3.1 Characterization of the Pt/MV-RGO-CH catalyst

The presence and distribution of Pt nanoparticles on MV-RGO-CH support were observed with TEM images shown in Fig. 1a. As shown in Fig. 1a, Pt nanoparticles were dispersed on MV-RGO-CH support very uniformly with very low agglomeration. This uniform dispersion was due to the presence of chitosan and methyl viologen in the support material. The mean particle size of Pt nanoparticles was

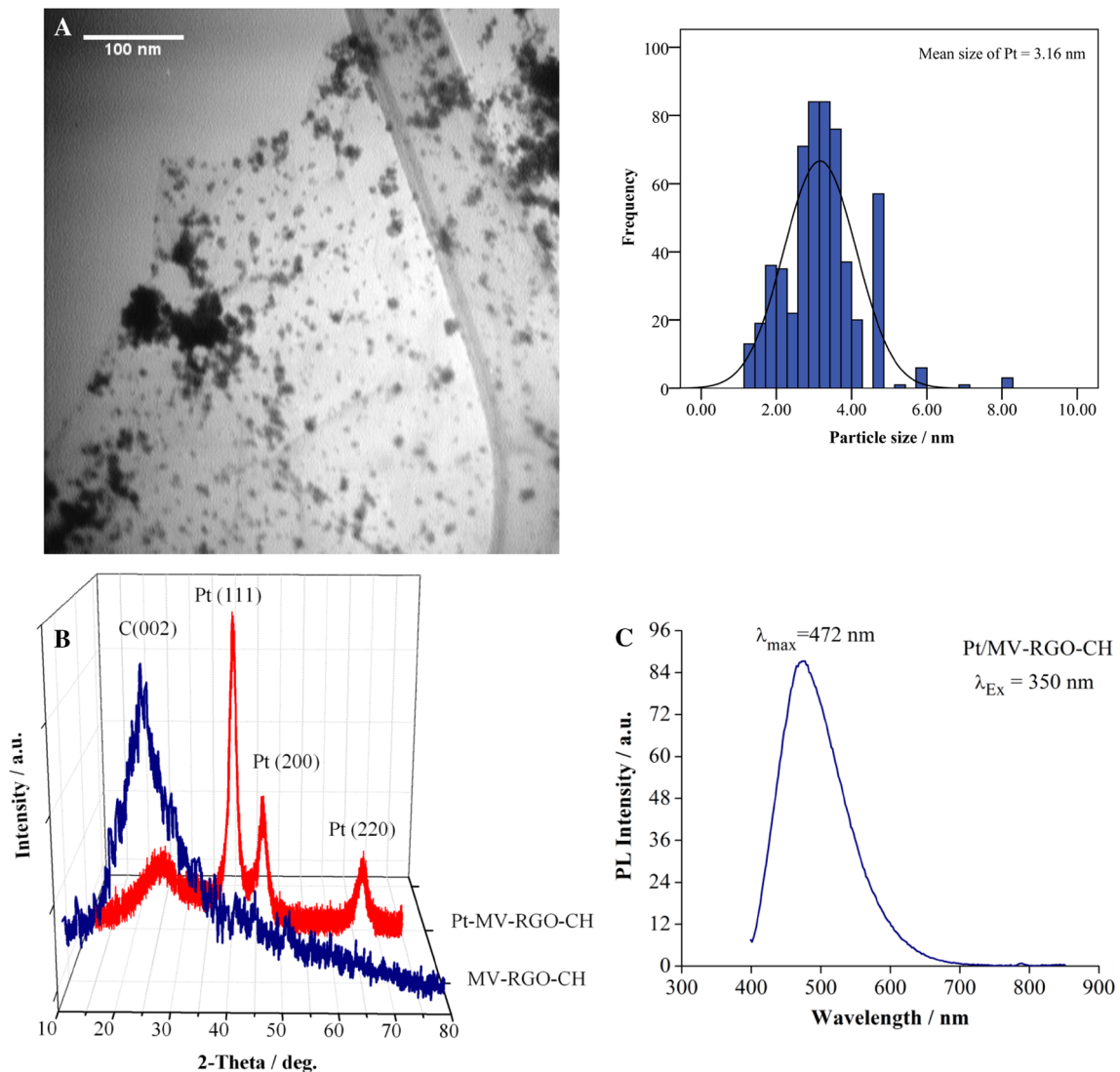


**Fig. 1** **a** TEM image of Pt/MV-RGO-CH catalyst, **b** XRD pattern of MV-RGO-CH and Pt/MV-RGO-CH and **c** photoluminescence emission of Pt/MV-RGO-CH at the corresponding excitation wavelength

3.16 nm. The presence of the amino group in chitosan (CH) facilitates the good dispersion of Pt nanoparticles. The amino group in chitosan is easily protonated to  $\text{NH}_3^+$  in acidic solution. Thus, there would be an electrostatic attraction between  $\text{PtCl}_6^{2-}$  (the precursor of Pt nanoparticles) and  $\text{NH}_3^+$  with the opposite charges. The electrostatic attractions between the positively charged functional groups of MV-RGO and CH polymer and the negatively charged  $\text{PtCl}_6^{2-}$  led to the very good dispersion of Pt nanoparticles.

The XRD patterns of MV-RGO-CH and Pt/MV-RGO-CH were shown in Fig. 1b. Pt/MV-RGO-CH catalyst indicated a broad diffraction peak centered at  $2\theta = 25^\circ$ , which corresponded to a d-spacing of 0.38 nm. This amount is close to the 0.33 nm d-spacing of graphite, showing that the most oxygen-containing functional groups of GO were removed by the reduction of GO to RGO with  $\text{NaBH}_4$  [41]. This diffraction peak is corresponded to C (002) of RGO which is clearly observed in the XRD pattern of MV-RGO-CH. At Pt/MV-RGO-CH catalyst, the diffraction peaks at  $39.8^\circ$ ,  $46.4^\circ$  and  $67.8^\circ$  are corresponded to the (111), (200), and (220) planes of the cubic structure of Pt, respectively [42].

Optical property of Pt/MV-RGO-CH catalyst was examined by photoluminescence (PL) spectrum (Fig. 1c). As shown in Fig. 1c, this catalyst has a broad peak. Under UV excitation at 350 nm, the maximum emission wavelength was 472 nm. Similar result was obtained by Sun and Sakka for PL of Pt catalyst [43].

### 3.2 Electrochemical studies

#### 3.2.1 Electrochemical active surface area and accelerated durability test of the prepared catalysts

Electrochemically active surface area (EAS) is an important factor to know the catalytic activity of Pt/MV-RGO-CH, Pt/MV-RGO and Pt/CH catalysts. EAS can be obtained by measuring  $\text{H}_2$  adsorption and desorption charges after double-layer correction and considering the  $0.21 \text{ mC cm}^{-2}$  value for adsorption of a hydrogen monolayer on Pt nanoparticles [44]. The CV curves of Pt/MV-RGO-CH electrode in the first and 50th potential cycles in  $0.5 \text{ M H}_2\text{SO}_4$  solution and the potential range of  $-0.35$  to  $1.2 \text{ V}$  were shown in Fig. 2a. The CV curves of Pt/MV-RGO-CH, Pt/MV-RGO and Pt/CH catalysts in  $0.5 \text{ M H}_2\text{SO}_4$  and the same potential range were also shown in Fig. 2b.

Coulombic charge ( $Q_H$ ) for hydrogen adsorption/desorption was used for calculating the EAS of catalysts [45]. The  $Q_H$  amount is considered as the mean value between the amounts of the charge exchanged during the electrochemically adsorption ( $Q''_H$ ) from  $-0.013$  to  $-0.25 \text{ V}$  versus SCE and desorption ( $Q'_H$ ) from  $-0.25$  to  $-0.011 \text{ V}$  versus SCE of hydrogen on Pt sites according to the following equation:

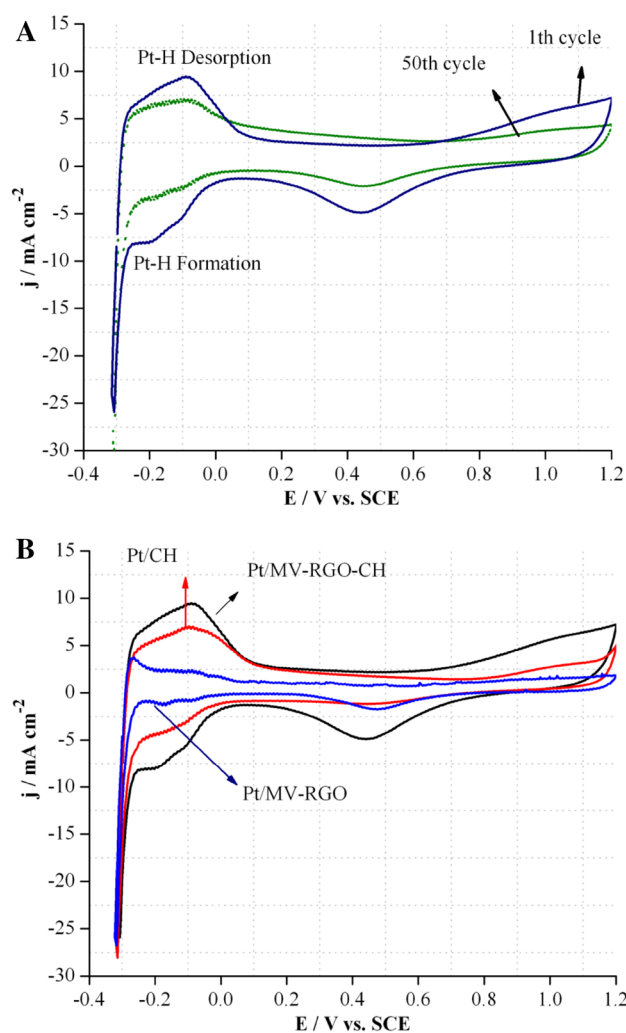


**Fig. 2** a CV curves of Pt/MV-RGO-CH in the first and 50th cycle, b CV curves of the prepared catalysts in  $0.5 \text{ M H}_2\text{SO}_4$

$$Q_H = \frac{(Q'_H + Q''_H)}{2} \quad (1)$$

The EAS for platinum can be calculated from Eq. (2) [46]:

$$\text{EAS} = \frac{Q_H}{0.21 \times [\text{Pt}]} \quad (2)$$

The calculated EAS for the prepared catalyst with the platinum loading [Pt] of  $0.041 \text{ mg cm}^{-2}$  with the scan rate of  $100 \text{ mV s}^{-1}$  was reported in Table 1. As presented in Table 1, among the prepared catalysts, the largest EAS was obtained at Pt/MV-RGO-CH catalyst ( $19.9 \text{ m}^2 \text{ g}^{-1}$ ) which was 1.5 times higher than that of Pt/CH ( $13.23 \text{ m}^2 \text{ g}^{-1}$ ) and 4.29 times higher than that of Pt/MV-RGO ( $4.63 \text{ m}^2 \text{ g}^{-1}$ ) catalyst, respectively. The larger EAS value of Pt/MV-RGO-CH catalyst shows that this

**Table 1** The calculated results from CV curves of the prepared catalysts in 0.5 M H<sub>2</sub>SO<sub>4</sub> aqueous solution at 100 mV s<sup>-1</sup>

Catalyst	No. cycle	EAS (m <sup>2</sup> g <sup>-1</sup> )	D <sub>Pt</sub>	% loss
Pt/MV-RGO-CH	1	19.9	0.026	28.64
Pt/MV-RGO-CH	50	14.2	0.019	
Pt/CH	1	13.23	0.017	
Pt/MV-RGO	1	4.63	0.0062	

catalyst has more active sites than Pt/CH and Pt/MV-RGO catalysts [45]. Also, this shows that the functionalization of RGO with MV and CH improves the dispersion of Pt nanoparticles [47].

Furthermore, dispersion of the Pt nanoparticles in the prepared catalysts can be shown by EAS. Dispersion of the Pt catalyst is known as the fraction of surface-active Pt atoms in all Pt atoms that can be estimated according to the following equation [48]:

$$D_{Pt} = \frac{EAS}{\frac{1}{M_{Pt}}(N_A, 4\pi r_{Pt}^2)} \quad (3)$$

M<sub>Pt</sub> is the relative molecular weight of Pt (195.08 g/mol), N<sub>A</sub> is Avogadro number (6.02 × 10<sup>23</sup>) and r<sub>Pt</sub> is the atomic ratio of Pt (0.139 nm). The obtained D<sub>Pt</sub> for Pt/MV-RGO-CH, Pt/CH, and Pt/MV-RGO catalysts in the first cycle were 0.026, 0.017, and 0.0062, respectively. Higher D<sub>Pt</sub> of the Pt/MV-RGO-CH catalyst showed that this catalyst has better dispersion of Pt nanoparticles than Pt/CH and Pt/MV-RGO catalysts.

Furthermore, accelerated durability test (ADT) of the Pt/MV-RGO-CH nanocatalyst was done in 0.5 M H<sub>2</sub>SO<sub>4</sub> by continuously applying potentials between -0.35 and 1.2 V with the scan rate of 100 mV s<sup>-1</sup> after 50 potential cycles. In general, the durability of GC/Pt/MV-RGO-CH electrode was investigated by performing potential cycling as ADT in H<sub>2</sub>SO<sub>4</sub> solution. The change of PtNPs electrochemical surface area for GC/Pt/MV-RGO-CH electrode was determined by comparing H<sub>2</sub> adsorption/desorption regions before and after 50 potential cycles (Fig. 2a). The EAS amount of GC/Pt/MV-RGO-CH electrode was decreased from 19.9 to 14.2 m<sup>2</sup> g<sub>Pt</sub><sup>-1</sup> after ADT. The obtained %ADT parameter (Table 1) was calculated according to the following equation [49]:

$$\% ADT = \frac{(EAS_{run1} - EAS_{run50})}{EAS_{run1}} \times 100 \quad (4)$$

%ADT was calculated 28.64% for GC/Pt/MV-RGO-CH electrode after 50 potential cycles. As can be seen in Table 1, D<sub>Pt</sub> value of the GC/Pt/MV-RGO-CH electrode decreases from 0.026 to 0.019 after ADT, indicating a

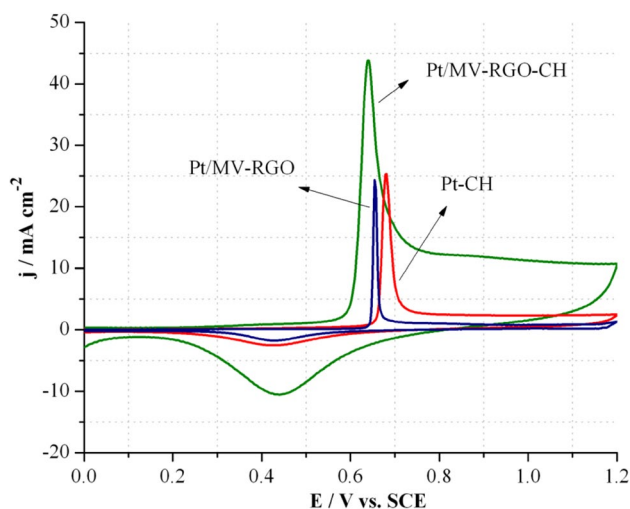


**Fig. 3** CO stripping voltammograms of the prepared catalysts in 0.5 M H<sub>2</sub>SO<sub>4</sub>

notable decrease in the active surface area of Pt nanoparticles due to Pt sintering.

### 3.3 CO stripping study

CO stripping experiments were done to investigate carbon monoxide (CO) oxidation properties and the CO tolerance ability of Pt/MV-RGO-CH, Pt/CH, and Pt/MV-RGO catalysts [50]. Figure 3 showed the adsorbed CO stripping curves of the prepared catalysts. For the CO oxidation experiment, CO was purged in 0.5 M H<sub>2</sub>SO<sub>4</sub> solution for 20 min in 0.2 V versus SCE. After the adsorption, N<sub>2</sub> gas was used for 30 min to remove CO from the electrolyte. All the prepared catalysts showed a sharp and single CO oxidation peak [51]. The peak potentials of Pt/MV-RGO-CH, Pt/CH, and Pt/MV-RGO catalysts for CO oxidation were 0.641, 0.681, and 0.654 V, respectively. The onset potential of CO oxidation at Pt/MV-RGO-CH catalyst (0.599 V) was more negative than that of Pt/CH (0.637 V) and Pt/MV-RGO (0.620 V) catalysts. The negative shift in the onset and peak potential of CO oxidation peak at Pt/MV-RGO-CH catalyst revealed that this catalyst has a higher CO tolerance and weaker interaction with CO than Pt/CH and Pt/MV-RGO catalysts [52, 53].

The EAS<sub>CO</sub> values of Pt/MV-RGO-CH catalyst was also determined using CO oxidation charges from 0.58 to 0.72 V of the CO stripping cure after subtracting the background current of the subsequent CV curve. The CO oxidation charge for Pt/CH and Pt/MV-RGO catalysts was calculated from 0.637 to 0.783 V and from 0.620 to 0.783 V, respectively. EAS<sub>CO</sub> was calculated by using the following equation [54] with the assumption of 420 μC cm<sup>-2</sup> as the

oxidation charge for one monolayer of CO on a smooth Pt surface [55].

$$EAS_{CO} = \frac{Q_{CO}}{G \times 420} \quad (5)$$

$Q_{CO}$  is the charge for CO desorption-electrooxidation in micro coulomb ( $\mu\text{C}$ ) and  $G$  is the Pt loading ( $\mu\text{g}$ ) on the electrode. The  $EAS_{CO}$  of Pt/MV-RGO-CH, Pt/CH, and Pt/MV-RGO catalysts were 16.56, 5.25, and  $2.49 \text{ m}^2 \text{ g}_{\text{Pt}}^{-1}$ , respectively. As seen,  $EAS_{CO}$  of the Pt/MV-RGO-CH catalyst was higher than those of the Pt/CH and Pt/MV-RGO catalysts. This confirmed the results of the EAS obtained from hydrogen adsorption and desorption.

### 3.3.1 Methanol oxidation reaction (MOR)

The electrocatalytic property of Pt/MV-RGO-CH, Pt/CH, and Pt/MV-RGO catalysts was studied for methanol electrooxidation through cyclic voltammetry (CV) in 1.83 M methanol and 0.5 M  $\text{H}_2\text{SO}_4$  aqueous solution at the scan rate of  $100 \text{ mV s}^{-1}$  (Fig. 4A). As no current peak of MO was seen in the CV of GC/MV-RGO-CH electrode (Fig. 4A(a)), this electrode showed no electrocatalytic activity for MO (CVs at GC/MV-RGO and GC/CH electrodes were not shown, which were similar to that of GC/MV-RGO-CH electrode).

All the CV curves of the Pt/MV-RGO (Fig. 4A(b)), Pt/CH (Fig. 4A(c)), and Pt/MV-RGO-CH (Fig. 4A(d)) catalysts showed two oxidation peaks for MO. The first anodic oxidation peak was observed in the forward scan ( $j_f$ ) which was attributed to methanol electrooxidation and the second oxidation peak was observed in the backward scan ( $j_b$ ). This peak was due to the oxidation of the corresponding intermediates produced during methanol electrooxidation [56]. For the Pt/MV-RGO-CH catalyst (Fig. 4A(d)), the first oxidation peak of MO was seen in the forward scan around 0.72 V ( $E_f$ ), whereas the second oxidation peak of MO was observed during the backward scan around 0.44 V ( $E_b$ ). The first peak current density ( $j_f$ ) for MO at Pt/MV-RGO-CH catalyst was  $143.32 \text{ mA cm}^{-2}$ , whereas the second peak current density in the backward scan ( $j_b$ ) was  $96.71 \text{ mA cm}^{-2}$  ( $j_f/j_b = 1.48$ ). As shown in Fig. 4A, Pt/MV-RGO-CH catalyst presented the highest peak current density among the prepared catalysts, indicating that this catalyst had better electrocatalytic activity for MO than that of Pt/MV-RGO and Pt/CH catalysts. The experimental data of methanol electrooxidation at the prepared catalysts was shown in Table 2. Although Pt/MV-RGO-CH catalyst had a little more positive onset potential and anodic peak potential than Pt/MV-RGO catalyst for MO, its anodic peak current density was significantly higher than Pt/MV-RGO. It showed that the presence of MV-RGO accompanied by chitosan significantly improved the electrocatalytic activity

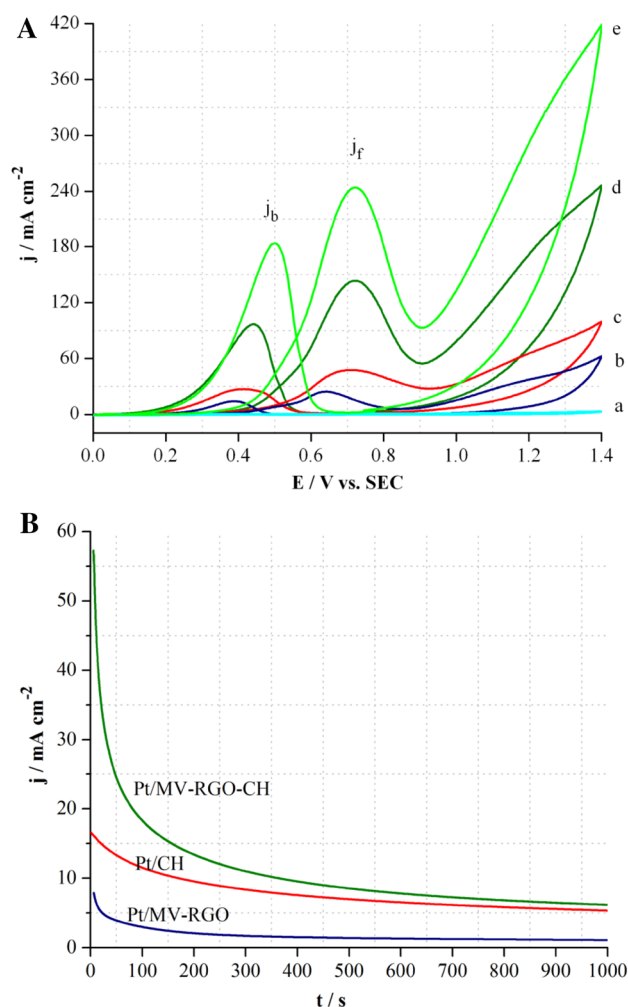
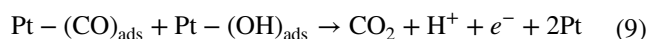
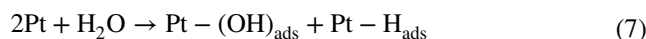
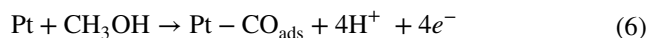


**Fig. 4** **A** Cyclic voltammograms of (a) MV-RGO-CH, (b) Pt/MV-RGO, (c) Pt/CH, (d) Pt/MV-RGO-CH no light, (e) Pt/MV-RGO-CH irradiated and **B** Chronoamperometric curves of the prepared catalysts for MO in 1.83 M methanol and 0.5 M  $\text{H}_2\text{SO}_4$

of Pt nanoparticles towards methanol electrooxidation. The mechanism of methanol oxidation at Pt catalyst can be as follows [57]:



The catalytic activity of Pt/MV-RGO-CH catalyst for MOR was also investigated in the absence and presence of irradiation. Figure 4A(d) showed the Pt/MV-RGO-CH activity for MO in the absence of irradiation, whereas Fig. 4A(e) indicated its catalytic activity in the presence of irradiation. A broad spectrum near-UV to infrared light

**Table 2** The experimental data of the prepared catalysts for MO in the absence of light in 1.83 M methanol and 0.5 M H<sub>2</sub>SO<sub>4</sub> aqueous solution at 100 mV s<sup>-1</sup>

Catalysts	Onset potential (V)	E <sub>f</sub> (V)	E <sub>b</sub> (V)	j <sub>f</sub> (mA cm <sup>-2</sup> )	j <sub>b</sub> (mA cm <sup>-2</sup> )
Pt/MV-RGO	0.3	0.65	0.39	24.08	14.08
Pt/CH	0.3	0.723	0.405	47.31	27.04
Pt/MV-RGO-CH	0.31	0.72	0.44	143.32	96.71

source was used for irradiation. In the presence of irradiation, methanol electrooxidation at Pt/MV-RGO-CH catalyst was enhanced. Anodic current density (j<sub>f</sub>) was increased from 143.32 to 243.98 mA cm<sup>-2</sup>. The same behavior was observed by Arulmani with Pt/C catalyst [58].

### 3.3.2 Amperometric i-t curve study

The long-term stability of Pt/MV-RGO-CH, Pt/CH, and Pt/MV-RGO catalysts for MOR was investigated by amperometric measurements in 0.5 M H<sub>2</sub>SO<sub>4</sub> and 1.83 M methanol solution at the constant potential of 0.7 V for 1000s (Fig. 4B). As shown in Fig. 4B, there was a rapid decrease in the potentiostatic current densities of all the catalysts in the initial stage. This decrease may be attributed to the reactive intermediates produced during MOR [59]. The initial current density of MO at Pt/MV-RGO-CH catalyst was 55.35 mA cm<sup>-2</sup>. After 200 s, the current density reached a constant value of 13.40 mA cm<sup>-2</sup>. For as long as 1000 s, the current density of MO at Pt/MV-RGO-CH catalyst remained at 6.17 mA cm<sup>-2</sup>. The initial current density of MO at Pt/CH catalyst was 16.60 mA cm<sup>-2</sup> and after 1000 s, it was 1.85 mA cm<sup>-2</sup>. At the Pt/MV-RGO catalyst, the initial current density was 7.89 mA cm<sup>-2</sup> and after 1000 s, it was 1.1 mA cm<sup>-2</sup>. It was noted that Pt/MV-RGO-CH catalyst had the highest steady state current density for MOR.

### 3.3.3 Electrochemical impedance spectroscopy (EIS) study

EIS studies were also performed to investigate the behavior of Pt/MV-RGO-CH, Pt/CH, and Pt/MV-RGO catalysts for MOR. Nyquist plot was used to investigate the electrochemical behavior of the prepared catalysts for methanol electrooxidation [60]. The electrochemical impedance study was done in the range of 1 × 10<sup>4</sup> to 10<sup>-2</sup> Hz at the open circuit potential (OCP) in 0.5 M H<sub>2</sub>SO<sub>4</sub> and 1.83 M methanol solution (Fig. 5). The Nyquist plots of all the catalysts were observed to have a very small semicircle in the high frequency region which is related to the charge transfer process in the interface of electrolyte and electrode

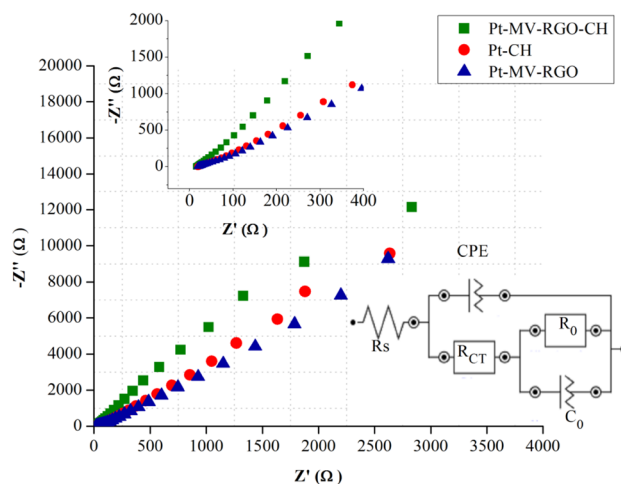


**Fig. 5** Nyquist plots of Pt/MV-RGO-CH, Pt/MV-RGO and Pt/CH catalysts in 0.5 M H<sub>2</sub>SO<sub>4</sub> and 1.83 M methanol aqueous solution

and a line in the low-frequency region which is due to the diffusion process in the prepared electrode. The equivalent circuit of the Pt/MV-RGO-CH catalyst was also indicated in the inset of Fig. 5. As seen in the circuit, R<sub>s</sub> is the solution resistance, CPE is the constant-phase element which is attributed to the double-layer capacitance. C<sub>0</sub> and R<sub>0</sub> are related to the capacitance and resistance of the adsorbed CO intermediates produced during methanol oxidation, respectively [61]. Among all the prepared catalysts, Pt/MV-RGO-CH showed a more vertical straight line and also a smaller value of the semicircle diameter indicating that this catalyst had faster kinetics of the ions diffusion process and faster charge transfer reaction rate for MOR [62].

### 3.3.4 Parameters affecting on MOR

Several parameters such as temperature, methanol concentration and scan rate influence the performance of Pt/MV-RGO-CH electrode for MOR. Hence, these parameters were studied and optimized.

To investigate the effect of temperature on the performance of Pt/MV-RGO-CH nanocatalyst towards MOR, the electrocatalytic activity of GC/Pt/MV-RGO-CH electrode was examined in different temperatures ranging from 23 to 50 °C (Fig. 6). As observed, the anodic current density was increased with the increase of temperature indicating that mass transport is an important factor for higher activity. As the temperature increased from 23 to 50 °C, j<sub>f</sub> increased from 134.88 to 323.42 mA cm<sup>-2</sup>. At the same methanol concentration (1.83 M methanol), the higher current density at the higher temperature shows that the fine structure of catalyst has more available Pt active sites for participating in the electrochemical

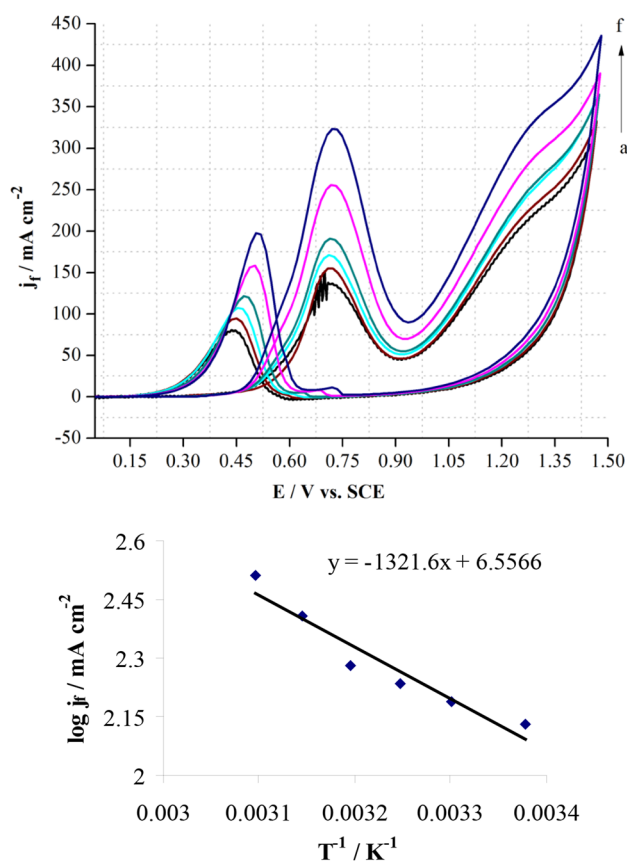


**Fig. 6** Cyclic voltammograms of Pt/MV-RGO-CH catalyst in different temperatures of (a) 23, (b) 30, (c) 35, (d) 40, (e) 45 and (f) 50 °C in 0.5 M H<sub>2</sub>SO<sub>4</sub> and 1.83 M methanol. The Arrhenius plot of logarithm of exchange current density ( $\log j_p$ ) versus the reciprocal of temperature ( $T^{-1}$ ) was also shown

reaction. The Arrhenius plot of logarithm of the exchange current density ( $\log j_p$ ) versus the reciprocal of temperature ( $T^{-1}$ ) was also indicated in Fig. 6.

The activation energy of the anodic peak of MO at the GC/Pt/MV-RGO-CH electrode was calculated from the following equation:

$$\frac{\partial \ln j_f}{\partial \left(\frac{1}{T}\right)} = \frac{\Delta H^*}{R} \quad (10)$$

The activation energy ( $\Delta H$ ) of the anodic peak of MO at the GC/Pt/MV-RGO-CH electrode was 10.987 kJ mol<sup>-1</sup>.

The catalytic activity of Pt/MV-RGO-CH catalysts towards MO was investigated at the different scan rates of 30, 60, 80, 100, 130, 160, and 190 mVs<sup>-1</sup> in 1.83 M methanol and 0.5 M H<sub>2</sub>SO<sub>4</sub> (Fig. 7). As shown in Fig. 7, the anodic peak current density of MO increased with increase of the applied scan rate. The linear relationship between the square root of scan rate ( $v^{0.5}$ ) and anodic peak current

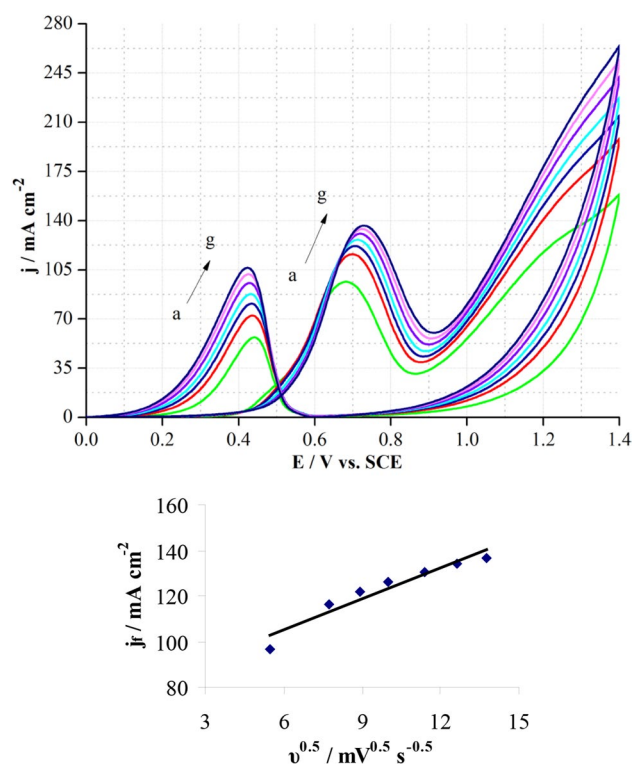


**Fig. 7** Cyclic voltammograms of Pt/MV-RGO-CH catalyst in 0.5 M H<sub>2</sub>SO<sub>4</sub> and 1.83 M methanol at different scan rates of (a) 30, (b) 60, (c) 80, (d) 100, (e) 130, (f) 160 and (g) 190 mV s<sup>-1</sup>. Anodic current density ( $j_p$ ) vs. square root of scan rate ( $v^{0.5}$ ) was also shown

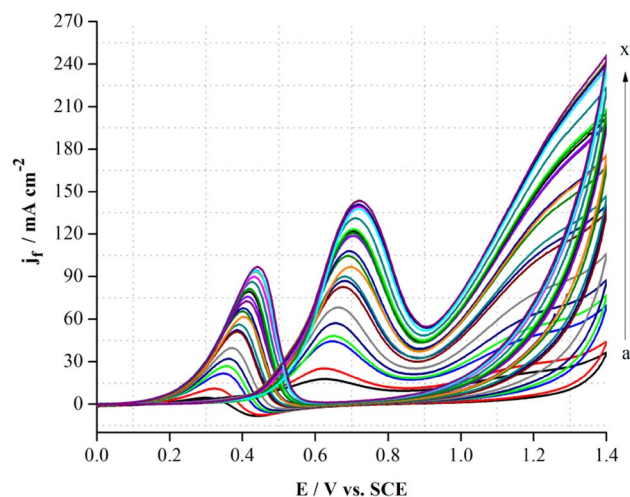


**Fig. 8** Cyclic voltammograms for MO on Pt/MV-RGO-CH electrode in 0.5 M H<sub>2</sub>SO<sub>4</sub> in different concentration of methanol: (a) 0.08, (b) 0.16, (c) 0.24, (d) 0.32, (e) 0.41, (f) 0.48, (g) 0.56, (h) 0.64, (i) 0.72, (j) 0.79, (k) 0.87, (l) 0.95, (m) 1.03, (n) 1.1, (o) 1.18, (p) 1.25, (q) 1.32, (r) 1.39, (s) 1.47, (t) 1.54, (u) 1.62, (v) 1.69, (w) 1.76 and (x) 1.83 M

density ( $j_p$ ) shows that MOR is controlled by the diffusion of methanol from the bulk solution to the electrode surface [63, 64].



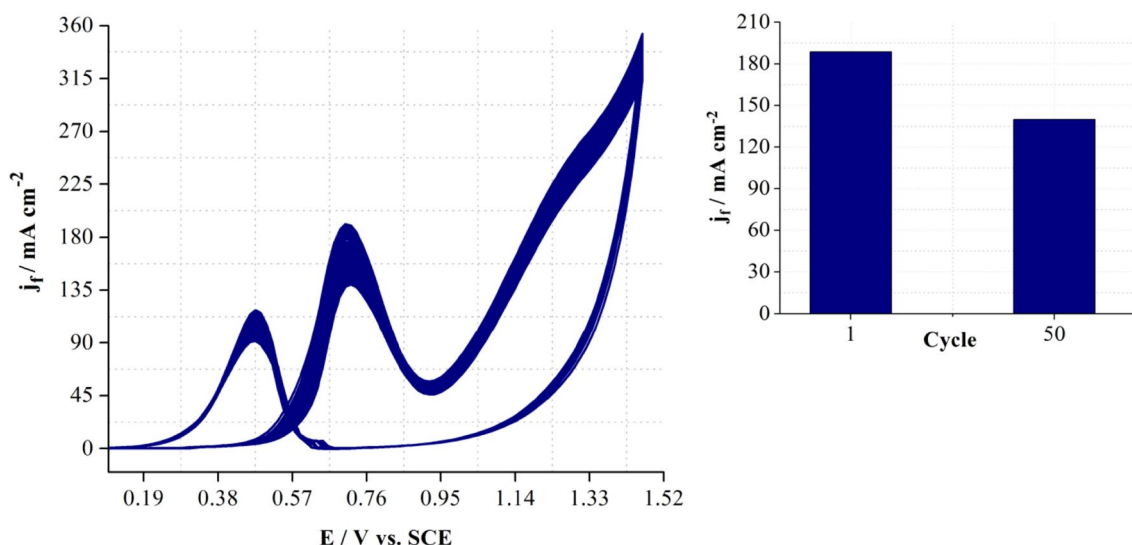


**Fig. 9** CV curve of Pt/MV-RGO-CH catalyst during the 50 cycles in  $\text{H}_2\text{SO}_4$  0.5 M and methanol 1.83 M solution.  $J_f$  of Pt/MV-RGO-CH catalyst as a function of the cycle number for MOR was also shown

The effect of methanol concentration on the anodic current density of MO on GC/Pt/MV-RGO-CH electrode was investigated in Fig. 8. As observed, anodic current density increases with increase in methanol concentration and levels off at concentrations higher than 1.83 M. This is probably because of the saturation of active sites on the surface of electrode. At the GC/Pt/MV-RGO-CH electrode, as methanol concentration increases from 0.08 to 1.83 M,  $E_f$  shifts towards a positive direction from 0.62 to 0.72 V. This probably occurs because of the increase in the poisoning rate of Pt catalyst. This means that the oxidative removal of the strongly adsorbed intermediates occurs at more positive potentials [65].

### 3.4 Durability investigation

The poisoning effect of GC/Pt/MV-RGO-CH electrode during MOR was studied through cyclic voltammetry with 50 cycles repeatedly (Fig. 9). At the GC/Pt/MV-RGO-CH electrode, in the first cycle,  $j_f$  was  $188.56 \text{ mA cm}^{-2}$  whereas it was  $139.81 \text{ mA cm}^{-2}$  in the 50th cycle. This showed that GC/Pt/MV-RGO-CH electrode had good durability for MOR.

## 4 Conclusions

In this research, a novel Pt/MV-RGO-CH nanocatalyst was successfully prepared and characterized. The electrocatalytic activity of the prepared catalyst was investigated for methanol electrooxidation and compared with that of Pt/CH and Pt/MV-RGO catalysts. The catalytic activity of

the prepared electrodes depends on the surface available for dispersion of the metallic particles. Pt/MV-RGO-CH catalyst showed higher electrocatalytic activity for MOR than Pt/CH and Pt/MV-RGO catalysts. This was due to its higher electrochemically active surface area, better anti-poisoning effect, good durability and higher anodic current for MO than the other two catalysts. The higher catalytic activity of Pt/MV-RGO-CH catalyst towards MO was because of the better dispersion of Pt nanoparticles. The presence of chitosan and methyl viologen on graphene sheets causes the good dispersion of nanoparticles and prevents agglomeration of the metallic particles. Also, the use of chitosan polymer in preparing Pt nanoparticles caused very good adherent of the catalyst suspension on the working electrode surface. By and large, these studies showed that Pt/MV-RGO-CH is a promising catalyst for MOR.

**Acknowledgements** We thank Esfarayen University of Technology for financial support.

## References

1. K. Kakaei, *Electrochim. Acta* **165**, 330 (2015)
2. M. Noroozifar, M. Khorasani-Motlagh, R. Khaleghian-Moghadam, M.-S. Ekrami-Kakhki, M. Shahraki, *J. Solid State Chem.* **201**, 41 (2013)
3. M. Winter, R.J. Brodd, *Chem. Rev.* **104**, 4245 (2004)
4. M.-S. Ekrami-Kakhki, Z. Yavari, J. Saffari, S. Abbasi, *J. Nanostruct.* **6**, 221 (2016)
5. D.A. Konopka, M. Li, K. Artyushkova, N. Marinkovic, K. Sasaki, R. Adzic, T.L. Ward, P. Atanassov, *J. Phys. Chem. C* **115**, 3043 (2011)

6. B. Fang, M. Kim, J.S. Yu. *Appl. Catal. B* **84**, 100 (2008)
7. Y. Shao, G. Yin, Y. Gao, P. Shi, J. Electrochem. Soc. **153**, A1093 (2006)
8. J. Lobato, P. Canizares, D. Ubeda, F.J. Pinar, M.A. Rodrigo, *Appl. Catal. B* **106**, 174 (2011)
9. C.T. Hsieh, J.Y. Lin, *J. Power Sources* **374**, 188 (2009)\*\*
10. H.L. Wang, B.A. Kakad, T. Tamaki, T. Yamaguchi, *J. Power Sources* **260**, 338 (2014)
11. R. Khaleghian-Moghadam, M. Noroozifar, M. Khorasani-Motlagh, M.-S. Ekrami-Kakhki, *J. Solid State Electrochem.* **17**, 643 (2013)
12. X. Li, H.J. Wang, H. Yua, Z.W. Liu, F. Peng, *J. Power Sources* **260**, 1 (2014)
13. M. Noroozifar, M. Khorasani-Motlagh, M.-S. Ekrami-Kakhki, R. Khaleghian-Moghadam, *J. Power Sources* **248**, 130 (2014)
14. H. Yang, C. Coutanceau, J.M. Léger, N. Alonso-Vante, C. Lamy, *J. Electroanal. Chem.* **576**, 305 (2005)
15. J. Lobato, P. Canizares, M.A. Rodrigo, J.J. Linares, R. López-Vizcaíno, *Energy Fuels* **22**, 3335 (2008)
16. S.S. John, I. Dutta, A.P. Angelopoulos, *Langmuir* **27**, 5781 (2011)
17. J. Qi, L. Jiang, S. Wang, G. Sun, *Appl. Catal. B* **107**, 95 (2011)
18. Y. Zhang, C. Liu, Y. Min, X. Qi, X. Ben, *J. Mater. Sci.* **24**, 3244 (2013)
19. Z.K. Ghouri, NAM. Barakat, P.S. Saud, M. Park, B.S. Kim, H.Y. Kim, *J. Mater. Sci.* **27**, 3894 (2016)
20. H. Zhang, X. Xu, P. Gu, C. Li, P. Wu, C. Cai, *Electrochim. Acta* **56**, 7064 (2011)
21. X.J. Zhou, P.H. Shi, Y.F. Qin, J.C. Fan, Y.L. Min, W.F. Yao, *J. Mater. Sci.* **27**, 1020 (2016)
22. Y. Liu, D. Zhang, *J. Mater. Sci.* **28**, 4965 (2017)
23. K. Kakaei, *Carbon* **51**, 195 (2013)
24. Y. Li, L. Han, B. An, Y. Wang, L. Wang, X. Yin, J. Lu, *J. Mater. Sci.* **27**, 6208 (2016)
25. K. Kakaei, H. Gharibi, *Energy* **65**, 166 (2014)
26. K. Vinodgopal, B. Neppolian, I.V. Lightcap, F. Grieser, M. Ashokkumar, P.V. Kamat, *J. Phys. Chem. Lett.* **1987**, 1 (2010)
27. H. Liu, J. Cao, M. Xue, N. Zhu, M. Zhang, T. Cao, *Langmuir* **25**, 12006 (2009)
28. O. Akyıldırım, H. Yükses, H. Saral, İ. Ermiş, T. Eren, M. Lütfi Yola, *Mater. Sci.* **27**, 8559 (2016)
29. D.R. Dreyer, S. Park, C.W. Bielawski, R.S. Ruoff, *Chem. Soc. Rev.* **39**, 228 (2010)
30. J. Zhao, H. Yu, Z. Liu, M. Ji, L. Zhang, G. Sun, *J. Phys. Chem. C* **118**, 1182 (2014)
31. S. Guo, S. Dong, E. Wang, *ACS Nano* **4**, 547 (2009)
32. S. Mayavan, H.S. Jang, M.J. Lee, S.H. Choi, S.M. Choi, *J. Mater. Chem. A* **1**, 3489 (2013)
33. F. Jafari, A. Salimi, A. Navaee, *Electroanalysis* **26**, 1782 (2014)
34. D.M. Zhou, J.J. Sun, H.Y. Chen, H.Q. Fang, *Electrochim. Acta* **43**, 1803 (1998)
35. J. Ma, L. Wang, X. Mu, Y. Cao, *J. Colloid Interface Sci.* **457**, 102 (2015)
36. S. Qudisia, M.I. Ahmed, Z. Hussain, S. Soomro, *J. Mater. Sci.* **1**, 1 (2017)
37. EHM. Sakho, O.S. Oluwafemi, S. Thomas, N. Kalarikkal, *J. Mater. Sci.* **28**, 2651 (2017)
38. M. Khorasani-Motlagh, M. Noroozifar, M.-S. Ekrami-Kakhki, *Int. J. Hydrog. Energy* **36**, 11554 (2011)
39. J.H. Ma, L. Wang, X. Mu, L. Li, *Int. J. Hydrog. Energy* **40**, 2641 (2015)
40. P. Zeng, R. Ran, Z. Chen, W. Zhou, H. Gu, Z. Shao, S. Liu, *J. Alloy Compd.* **465**, 455 (2008)
41. H.J. Shin, K.K. Kim, A. Benayad, S.M. Yoon, H.K. Park, I.S. Jung, M.H. Jin, H.K. Jeong, J.M. Kim, J.Y. Choi, Y.H. Lee, *Adv. Funct. Mater.* **19**, 1987 (2009)
42. C.C. Kung, P.Y. Lin, Y. Xue, R. Akolkar, L. Dai, X. Yu, C.C. Liu, *J. Power Sources* **329**, 256 (2014)
43. H.T. Sun, Y. Sakka, *Sci. Technol. Adv. Mater.* **15**, 014205 (2014)
44. Z. Yan, H. Wang, M. Zhang, Z. Jiang, T. Jiang, J. Xie, *Electrochim. Acta* **95**, 218 (2013)
45. X. Zhang, B. Zhang, D. Liu, J. Qiao, *Electrochim. Acta* **177**, 93 (2015)
46. K. Kakaei, A. Rahimi, S. Husseindoost, M. Hamidi, H. Javan, A. Balavandi, *Int. J. Hydrog. Energy* **41**, 3861 (2016)
47. H. Zhang, X. Bo, L. Guo, *Electrochim. Acta* **201**, 117 (2016)
48. C. Zhou, Y. Chen, Z. Guo, X. Wang, Y. Yang, *Chem. Commun.* **7473**, 47 (2011)
49. M. Noroozifar, Z. Yavari, M. Khorasani-Motlagh, T. Ghasemi, S.-H. Rohani-Yazdi, M. Mohammadi, *RSC Adv.* **563**, 6 (2016)
50. J. Sun, M. Dou, Z. Zhang, J. Ji, F. Wang, *Electrochim. Acta* **447**, 215 (2016)
51. F. Alcaide, G. Alvarez, P.L. Cabot, H.J. Grande, O. Miguel, A. Querejeta, *Int. J. Hydrog. Energy* **36**, 4432 (2011)
52. Z. Yang, A. Nagashima, T. Fujigaya, N. Nakashima, *Int. J. Hydrog. Energy* **41**, 19182 (2016)
53. S. Moniri, T. Van Cleve, S. Linic, *J. Catal.* **345**, 1 (2017)
54. Z.B. Wang, G.P. Yin, J. Zhang, Y.C. Sun, P.F. Shi, *J. Power Sources* **160**, 37 (2006)
55. Y. Hao, X. Wang, Y. Zheng, J. Shen, J. Yuan, A. Wang, L. Niu, S. Huang, *Int. J. Hydrog. Energy* **41**, 9303 (2016)
56. M.-S. Ekrami-Kakhki, M. Khorasani-Motlagh, M. Noroozifar, *J. Appl. Electrochem.* **41**, 527 (2011)
57. P. Gajendran, R. Saraswathi, *J. Solid State Chem.* **17**, 2741 (2013)
58. D.V. Arulmani, J.I. Eastcott, S.G. Mavilla, E. Bradley Easton, *J. Power Sources* **247**, 890 (2014)
59. S.K. Meher, R.G. Ranga, *ACS Catal.* **2**, 2795 (2012)
60. K. Ding, Z. Jia, Q. Wang, X. He, N. Tian, R. Tong, X. Wang, *J. Electroanal. Chem.* **513**, 67 (2001)
61. Q. He, W. Chen, S. Mukerjee, S. Chen, F. Laufek, *J. Power Sources* **187**, 298 (2009)
62. M.Q. Hao, X.H. Liu, M.N. Feng, P.P. Zhang, G.Y. Wang, *J. Power Sources* **251**, 222 (2014)
63. K. Honda, M. Yoshimura, T.N. Rao, D.A. Tryk, A. Fujishima, K. Yasui, Y. Sakamoto, K. Nishio, H. Masuda, *J. Electroanal. Chem.* **514**, 35 (2001)
64. Y. Zhao, R. Wang, Z. Han, C. Li, Y. Wang, B. Chi, J. Li, X. Wang, *Electrochim. Acta* **151**, 544 (2015)
65. Z. He, J. Chen, D. Liu, H. Zhou, Y. Kuang, *Diam. Relat. Mater.* **13**, 1764 (2004)